ADVANCES IN ROTORCRAFT SIMULATIONS WITH UNSTRUCTURED CFD

Jennifer N. Abras* C. Eric Lynch† Marilyn J. Smith‡
Georgia Institute of Technology
Atlanta, Georgia 30332-0150

Abstract

Advances have been made in the development of unstructured solver methods suitable for fixed wing analyses, as well as rotary-wing applications, including interaction aerodynamics. This paper demonstrates the ability of an unstructured overset solver, FUN3D, to resolve the viscous compressible equations of motion for rotor-fuselage interactions and rotor-alone configurations. The solver is capable of modeling fully-articulated rotors (prior work was limited to rotation and flapping) and CFD-CSD loosely-coupled solutions including trim, using overset approaches. Initial results with the UH60A rotor indicate that the unstructured solver provides similar loading to its structured solver counterparts. Additional development of efficient domain connectivity interface routines are warranted to provide the ability to perform tightly-coupled rotor simulations.

Nomenclature

a	axis of rotation
A	rotor disk area
c	center of rotation
C_T	thrust coefficient, $C_T = \frac{T}{(0.5\rho_\infty A\Omega^2 R^2)}$
C_p	pressure coefficient, $C_p = \frac{p-p_\infty}{(0.5\rho_\infty V^2)}$
M_x	roll moment, ft-lbs
M_y	pitch moment , ft-lbs
M_z	yaw moment , ft-lbs
r	radial coordinate
R	rotor blade radius
T	rotor thrust
u, v, w	velocity in the x, y, z Cartesian directions, respectively
V	velocity vector, $(u, v, w)^T$
x, y, z	Cartesian components in the stream, side and normal directions, respectively
X, Y, Z	Cartesian components in the stream, side and normal directions, respectively, nondimensionalized by reference length, L

Greek

α	angle of attack
β	blade flap angle, $\beta = \beta_0 + \beta_{1s}sin\psi + \beta_{1c}cos\psi$
δ	lead–lag angle
ρ	fluid density
ψ	blade azimuth angle
μ	advance ratio, $\mu = \frac{V_\infty}{\Omega R}$
ω	nondimensional vorticity
Ω	rotor rotational velocity
σ	solidity
θ	blade pitch angle, $\theta = \theta_0 + \theta_{tw}\frac{r}{R} + \theta_{1s}sin\psi + \theta_{1c}cos\psi$

*PhD Candidate and Graduate Research Assistant, School of Aerospace Engineering. Student Member, AHS. E-mail: gtg503s@mail.gatech.edu

†PhD Candidate and Graduate Research Assistant, School of Aerospace Engineering. Student Member, AHS. E-mail: gte258v@mail.gatech.edu

‡Associate Professor, Member, AHS. E-mail: marilyn.smith@ae.gatech.edu

Presented at the American Helicopter Society 63rd Annual Forum, Virginia Beach, VA, May 1-3, 2007.

Subscripts

s	shaft
T	tip
0	mean or root
$1s$	1st cyclic sine coefficient
$1c$	1st cyclic cosine coefficient
∞	free stream

Introduction

Accurate, yet efficient prediction of rotary-wing airloads has been a topic of interest for the past twenty to thirty years within the rotorcraft community. The rotor flow field is a complex interaction of unsteady viscous-dominated subsonic and transonic aerodynamics, that is further complicated via interactions with the flexible rotor blade. The wake system that develops from the lifting blade shed wake can remain in the near-field of the rotor and fuselage, introducing additional unsteady loading. Thus an accurate prediction of the airloads on a rotary-wing vehicle relies on the accurate prediction of the rotor structural dynamics, wake geometry, and unsteady aerodynamics, including vortex-surface interactions.

This dichotomy has yielded two lines of aerodynamics research in an attempt to resolve accuracy and computational expense. A detailed discussion of the history of the development of airloads numerical methods can be found in Refs. 1 and 2; a short synopsis of the state of the art is presented here for the reader.

The focus of practical computations for many years has been on the development of comprehensive codes characterized by the finite-element structural methods combined with efficient, low-fidelity aerodynamics and trim models. The aerodynamic models for these methods are typically chosen from lifting-line, dynamic inflow, and prescribed or free wake simulation techniques. Among the most popular of these codes are UMARC (Ref. 3), CAMRAD II (Ref. 4), DYMORE (Ref. 5), and HOST (Ref. 6). Kunz (Ref. 2) has presented a detailed discussion of the current capabilities of these comprehensive codes, with the exception of the HOST code.

As computational hardware has matured with affordable options such as highly-parallelized Linux clusters, the viability of computational fluid dynamics (CFD) methods to provide detailed airloads analysis has become a realistic option in production environments. Applications of CFD to rotorcraft have, in the past, yielded airloads that were inadequate for engineering utilization due to the lack of accurate aeroelastic blade response, poor wake resolution, and the inability to model complex configurations. These deficiencies have been addressed via a number of improvements. First, the coupling of CFD with computational structural dynamics (CSD) codes now permits the modeling of the articulated rotor with elastic response. This is not a new idea. As early as the 1980s, full-potential aerodynamic methods have been coupled with comprehensive codes (Ref. 7), with some success, but continuing problems resolving the pitching moments have limited the usefulness of full-potential methods. In the early 1990s, Smith (Ref. 8) coupled an Euler Navier-Stokes method with the nonlinear beam model of Hodges and Dowell (Ref. 9), but grid resolution due to computational memory limitations was still a concern.

More recently, using the impetus of the UH60A airloads workshop, CFD-CSD coupling has enjoyed a resurgence, this time with much better results due to the improvement in computational power. Using a loosely-coupled approach for level flight, a number of CFD methods have been successfully coupled with comprehensive codes, such as CAMRAD-OVERFLOW (Ref. 10), DYMORE-OVERFLOW (Ref. 11), RCAS-OVERFLOW (Ref. 12), UMARC-TURNS (Ref. 13), and HOST-elsA (Ref. 14).

These CFD solvers typically resolve the Reynolds-Averaged Navier Stokes (RANS) equations, and are formulated using three distinct grid-topologies. Most RANS codes utilize a structured scheme, since the natural ordering of the nodes reduces the required memory and solution time. However, creating a structured grid can take weeks for very complex configurations. Chimera and/or overset grids partially alleviate this problem, and their success in resolving complex rotorcraft is well documented (for example, Refs. 10 and 14). Initial research to apply Cartesian-based structured grid methods is also underway (Ref. 15), although recent research has focused on utilizing these methods with adaptive mesh refinement (AMR) capabilities for wake refinement, coupled with more mature solvers for the near-field simulations. Unstructured grid techniques offer the advantage of reduced grid generation time, along with the ability to make rapid configuration changes. With the recent advances in parallel computing, the increased overhead per node required by unstructured methods is no longer as important an issue, and the additional run time per node can be partially compensated by reduced grid density in areas far from the vehicle. Much of the focus with unstructured methodologies has been for the resolution of complex fuselage geometries and rotor-fuselage interactions, as illustrated in Refs. 15, 16, 17, 18 and 19 .

Rotor-fuselage interaction computational fluid dynamics (CFD) methods have focused primarily lower-fidelity rotor modeling, as the emphasis has been on predicting the fuselage loading. This lower-fidelity modeling usually takes the form of a rotor actuator disk, where discrete sources are inserted into the grid with magnitudes that include the influence of the rotor, obtained typically from momentum or blade element theory or a comprehensive code. New implementations include a closed feedback loop that permit interaction between the rotor and fuselage. This modeling has been shown to be accurate when steady airloads are required for fuselage design and analysis (e.g, Refs. 16, 20, and 21), and unsteady actuator blades appear to hold promise for unsteady fuselage loading (Refs. 16, 22).

These simulations appear to be sufficient if the emphasis is on fuselage loading. However, the most physically correct analysis requires that all surfaces be accurately modeled via the time-accurate Navier-Stokes equations. Full RANS rotor modeling adds a level of additional complexity since each rotor requires a rotating frame and the fuselage requires a stationary frame, which must co-exist within the simulation. Two methodologies have emerged for mixed frame problems using unstructured methods: overset and/or chimera grids, and sliding boundaries. Park and Kwon (Refs. 23, 24) have demonstrated via the Euler equations, the solution of a rotating main rotor cylindrical grid that fits within a background rectangular grid that contains the fuselage and remainder of the control volume. The two grids communicate via a sliding boundary that forms the interface between the two grids. The primary drawback to this approach is the restriction imposed on the type of configurations that can be modeled. Multiple overlapping rotors, such as compound rotors, cannot be modeled. The second approach utilizes a combination of overset or chimera grids to generate smaller grids around each rotor blade, which then rotate through a background Cartesian or unstructured grid, as illustrated in Fig.1 from Ref. 16. This overset approach, utilizing structured grids has been used to correctly capture the general experimental trends on several configurations by Hariharan (Ref. 21), Potsdam et al (Ref. 10) and Duque (Ref. 25). Recent publications by OBrien and Smith (Ref. 22) and O'Brien (Ref. 16) have demonstrated this technology utilizing an unstructured method for the solution of the compressible RANS equations to resolve fuselage loading.

This paper extends these unstructured demonstrations of O'Brien and Smith to include overset rotors with full rigid body motion and introduces CFD-CSD coupling concepts for unstructured grids. Emphasis here includes not only the fuselage loading reported earlier, but also explores the ability of the unstructured methods to correctly capture blade loading via correlation with experimental data and structured computational results (OVERFLOW).

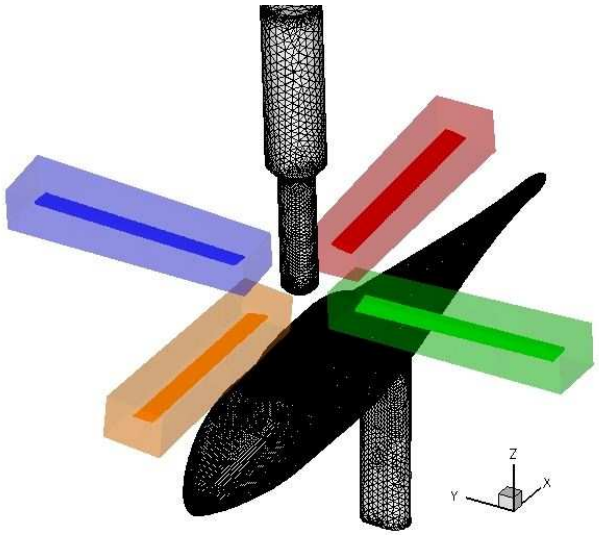

Figure 1: Robin rotor–fuselage unstructured overset grid (Ref. 16).

Methodology

This section first provides a short review of the baseline computational aerodynamic and structural dynamics methodologies, as well as the libraries that are utilized to effect the overset coupling.

Unstructured Methodology: FUN3D

The unstructured methodology that is utilized and extended within this effort is the FUN3D code developed at the NASA Langley Research Center (Ref. 26, 27, and 28). FUN3D can resolve either the compressible or incompressible RANS equations on unstructured tetrahedral meshes. The incompressible RANS equations are simulated via Chorin's artificial compressibility method (Ref. 29). A first-order backward Euler scheme with local time stepping has been applied to steady-state applications, while a second-order backward differentiation formula (BDF) has been utilized for time-accurate simulations. A point-implicit relaxation scheme resolves the resulting linearized system of equations. FUN3D solves the RANS equations on the non-overlapping control vol-

umes surrounding each cell vertex or node where the flow variables are stored. Inviscid fluxes on the cell faces are computed via Roes flux-difference-splitting scheme (Ref. 30), while viscous fluxes are computed with a finite volume formulation to obtain an equivalent central-difference approximation.

The FUN3D methodology was originally developed for fixed-wing applications. It has been extended to evaluate rotary-wing applications of interest by O'Brien and Smith (Refs. 16, 15, 20, 22). It has been shown by these researchers that FUN3D's incompressible formulation is not only robust for low-speed flight regimes, but results comparable to structured methods are obtained when the grids are locally comparable on the surface and boundary region. During these studies on rotor-fuselage interactions, an overset formulation of FUN3D was developed for comparison of lower-fidelity rotor models.

Overset Rotor Blade Model

Overset grid modeling in FUN3D is achieved using the Donor Interpolation Receptor Transaction Library (DiRTlib) (Ref. 31) library and Structured, Unstructured, and Generalized overset Grid AssembleR (SUGGAR) (Ref. 32) code, developed at ARL by Dr. Ralph Noack. DiRTlib provides a library of interface function that enable the flow solver perform overset computations without major modifications to the solver. DiRTlib's primary function is to interpolate the data at the fringes of the component meshes using the domain connectivity information (DCI) generated by the grid assembly program, SUGGAR. SUGGAR generates a single composite grid from the individual grids by determining the nodes in each domain (grid) that need to be blanked, and it identifies the locations where flow information needs to be interpolated. These interpolation node locations are stored in data connectivity interpolation (DCI) files. As SUGGAR is a stand-alone code, interactions between SUGGAR and the solver can be problematic. Prior to this work, the rigid rotor blade motions for each test case were known prior to the run, and the motion was simulated by a reduced set of rigid blade motion equations (flap without blade offsets) to the FUN3D solver as required. Prior to each FUN3D run, the DCI files for the known time increment for each iteration were pre-computed and stored in the run directory. This process is adequate (though not optimum) if only a reduced set of rigid blade motions is needed.

Nonlinear Elastic Multibody Dynamics: DYMORE

In order to facilitate the CFD-CSD coupling that is described later in this work, a CSD methodology needed to be selected. The code selected for this demonstration is the DYMORE code, developed at Georgia Tech (Ref. 5). DYMORE is a multibody finite element analysis code that can be applied to arbitrary nonlinear elastic systems, and has been proven in recent work (Ref. 11) using the OVERFLOW methodology as a suitable CSD methodology for CFD-CSD coupling. DYMORE includes an extensive library of multibody components that can be utilized to model mechanical components of a rotor system. This library is comparable to the component libraries in popular finite element methods for nonlinear elastic structural dynamics analysis. DYMORE can be applied to new topological designs with existing library elements or by the addition of new elements. Its modular approach allows the basic components to be validated independently. For flexible structures, DYMORE applies geometrically exact finite elements along the blades with limiting assumptions of the deflection values. It includes elements based on the work of Berdichevsky (Ref. 33), as extended to beams (Ref. 34) and shells (Ref. 35), which are very important for composite rotors and fuselage components.

Aerodynamically, DYMORE includes internal unsteady 2D airfoil computations, as well as options to utilize airloads from an external source, such as a CFD methodology. Trimming is achieved using an auto pilot method (Ref. 36), which has been successfully utilized in CFD-CSD couplings with OVERFLOW (Ref. 11) and a free wake methodology (Ref. 37). This method controls the zeroth and first harmonics of the blade pitching function via a reference jacobian matrix and three perturbations to compute function gradients. The function gradients are computed with the lower-fidelity aerodynamic methods found in DYMORE. Trim targets are achieved by applying the gradients along with the computed loads in DYMORE's aerodynamic model plus the frozen delta between the input higher-fidelity and lower-fidelity loads.

Advances in the Unstructured Overset Techniques

Fully-Articulated Rotor Motion

As previously discussed, in prior demonstrations of the unstructured overset methodology, rotor blade motion was limited to rotation and blade flapping referenced to the hub (center of rotation). This has been extended to allow fully-articulated motion where flap, pitch and lead-lag motion, along with hinge offsets, are modeled. Collective changes to effect trim convergence are also permitted. These motions are implemented via Fourier coefficients to prescribe the periodic motion of each degree of freedom, and then applying these coefficients to harmonically reconstruct the motion at each time step. The hinge offsets are included through the computation of the center of rotation of each degree of freedom. Finally, using the combination of center of rotation, axis of rotation, and angle of rotation, a set of transformation matrices is obtained which through matrix multiplication is combined to form one transformation matrix to specify the motion of each rotor blade: The RBM equations are computed in steps. The first step is to determine the axes of rotation and their corresponding centers of rotation. These will be denoted as $\vec{a}_\eta$ and $\vec{c}_\eta$, where η is a place holder for the rotation type of interest. The matrix that defines the rotation of the system about a specific axis will be denoted as A_η and is defined as,

$$A_\eta = \left[\begin{array}{c} (1-cos(\eta)) * a_{\eta x}^2 + cos(\eta) \\ (1-cos(\eta)) * a_{\eta x} * a_{\eta y} + sin(\eta) * a_{\eta z} \\ (1-cos(\eta)) * a_{\eta x} * a_{\eta z} - sin(\eta) * a_{\eta y} \end{array} \right. \quad \ldots$$

$$\begin{array}{c} (1-cos(\eta)) * a_{\eta x} * a_{\eta y} - sin(\eta) * a_{\eta y} \\ (1-cos(\eta)) * a_{\eta y}^2 + cos(\eta) \\ (1-cos(\eta)) * a_{\eta x} * a_{\eta y} + sin(\eta) * a_{\eta x} \end{array} \quad \ldots$$

$$\left. \begin{array}{c} (1-cos(\eta)) * a_{\eta x} * a_{\eta z} + sin(\eta) * a_{\eta y} \\ (1-cos(\eta)) * a_{\eta y} * a_{\eta z} - sin(\eta) * a_{\eta x} \\ (1-cos(\eta)) * a_{\eta z}^2 + cos(\eta) \end{array} \right] \quad (1)$$

The centers of rotation and axes of rotation are defined for this specific case to include the contributions of hinge offsets and shaft tilt :

$$\begin{array}{rcl} \vec{a}_\psi & = & (-sin(-\alpha_s) * sn, 0.0, cos(-\alpha_s) * sn) \\ \vec{c}_\psi & = & (x0, y0, z0) \\ \vec{a}_\theta & = & (cos(-\alpha_s) * sn, 0.0, sin(-\alpha_s) * sn) \\ \vec{c}_\theta & = & (x0 + PH * cos(-\alpha_s), y0, z0 + \\ & & PH * sin(-\alpha_s)) \\ \vec{a}_\delta & = & (-sin(-\alpha_s), 0.0, cos(-\alpha_s)) \\ \vec{c}_\delta & = & (x0 + LH * cos(-\alpha_s), y0, z0 \\ & & + LH * sin(-\alpha_s)) \\ \vec{a}_\beta & = & (0.0, -1.0, 0.0) \\ \vec{c}_\beta & = & (x0 + FH * cos(-\alpha_s), y0, z0 \\ & & + FH * sin(-\alpha_s)) \end{array}$$

Where (x_0, y_0, z_0) is the hub center, PH, FH, LH are the pitch, flap, and lag hinges of the rotor, and α_s is the shaft tilt angle. The variable sn is either 1 or -1 depending on the direction of rotation of the rotor. The angles are computed by reconstructing user input fourier coefficient data:

$$\begin{array}{rcl} \beta & = & \beta_0 + \beta_{1s} * sin(\psi) + \beta_{1c} * cos(\psi) + ... \\ \theta & = & \theta_0 + \theta_{1s} * sin(\psi) + \theta_{1c} * cos(\psi) + ... \\ \delta & = & \delta_0 + \delta_{1s} * sin(\psi) + \delta_{1c} * cos(\psi) + ... \end{array}$$

The total rotation matrix is then constructed by the set of sequential equations,

$$\begin{array}{rcl} R' & = & A_\theta I \\ R'' & = & A_\delta R' \\ R''' & = & A_\beta R'' \\ R^{tot} & = & A_\psi R''' \end{array}$$

Where R',R'',R''' are intermediate steps and R^{tot} is the total rotation matrix. The corresponding displacements are finally computed as,

$$\begin{array}{rcl} \vec{dx} & = & -A_\theta(\vec{c}_\theta) + \vec{c}_\theta \\ \vec{dx}'' & = & A_\delta(\vec{dx}' - \vec{c}_\delta) + \vec{c}_\delta \\ \vec{dx}''' & = & A_\beta(\vec{dx}'' - \vec{c}_\beta) + \vec{c}_\beta \\ \vec{dx}^{tot} & = & A_\psi(\vec{dx}''' - \vec{c}_\psi) + \vec{c}_\psi \end{array}$$

Where $\vec{dx}'$,$\vec{dx}''$,$\vec{dx}'''$ are intermediate steps and $\vec{dx}_{tot}$ is the resulting displacement vector. These components are used to relate the initial point to the deformed point as follows,

$$\vec{x}^{new} = R^{tot}\vec{x}^{old} + \vec{dx}^{tot} \quad (2)$$

This expression is applied to every grid point in the grid attached to the flexible surface at each time step, resulting in fully-articulated rotor motion.

Rigid blade motions are implemented by an input deck that permits the user to define the motion via

a set of motion commands. For example, blade pitch motion is achieved using the equation of motion:

$$\theta = \theta_0 + \theta_{1s} sin\psi + \theta_{1c} cos\psi \quad (3)$$

where the user inputs the coefficients $\theta_0, \theta_{1s}, \theta_{1c}$ that are applied within the rotor module of FUN3D.

Elastic blade motions are implemented slightly differently. The user will still input the rotor motion coefficients so that the basic rotor motion is properly updated in the blade motion routines. The elastic rotor motion is updated from a file that contains both the blade deflections and rigid motions. This file is output from DYMORE, and is formatted using the standard proposed by Nygaard et al (Ref. 38) so that the selection of the CSD module is not limited to DYMORE.

CFD–CSD Coupling

Prior to this effort, FUN3D already included the capability for aeroelastic flexibility via NASTRAN, however rotorcraft have specialized concerns in this area. Using comprehensive or multi-body dynamics codes, the rotor is typically modeled as one or more beams that must include not only the elastic beam deflections, but rigid body motion as well, so that the rotor may be trimmed to approximate the correct performance. The coupling process is being demonstrated with DYMORE, which has been successfully coupled at Georgia Tech to OVERFLOW (Ref. 11). A delta loads trim process, which has become a de facto standard among the rotorcraft community, is being utilized in this work.

Once elastic blades are introduced into the system, the overset methodology becomes much more complex. At every time step, a new DCI file that has been updated with the blade deflections is needed. Depending on the coupling strategy, this may require that SUGGAR be called and instructed to generate the new DCI file for the next time step. When SUGGAR finishes, the flow solver can advance the solution to the new time step.

One way around this problem is to apply a loose-coupling strategy. In rotorcraft applications, loose coupling has been taken to mean that loads and deflections data are exchanged for an entire rotor revolution, as illustrated in Fig. 2. First, the initialization of the trimmer jacobian and initial deflections is computed in DYMORE. The blade deflections are passed to FUN3D, which has been coupled with SUGGAR to generate a composite grid using the deflections and connectivities via the DCI files. These DCI files and composite grid are then passed to FUN3D where the run is integrated for some fraction of a revolution until the blade loading over a revolution is periodic. The azimuth fraction discussed above depends on the number of blades and the number of time steps required to reach a periodic solution. To illustrate, consider a four-bladed rotor, such as the UH60A. The minimum length of time that the CFD code needs to be run is $\frac{1}{4}$ of a revolution, as this fraction multiplied by the four blades is equivalent to a full revolution. If the loads at each quarter-revolution do not match at the boundaries, then the CFD simulation must be run for another quarter-revolution. This must be repeated until the loads are repeatable and have (near) C^o continuity at the run boundaries (e.g., for a four-bladed rotor at $0^o, 90^o, 180^o, 270^o$, and 360^o).

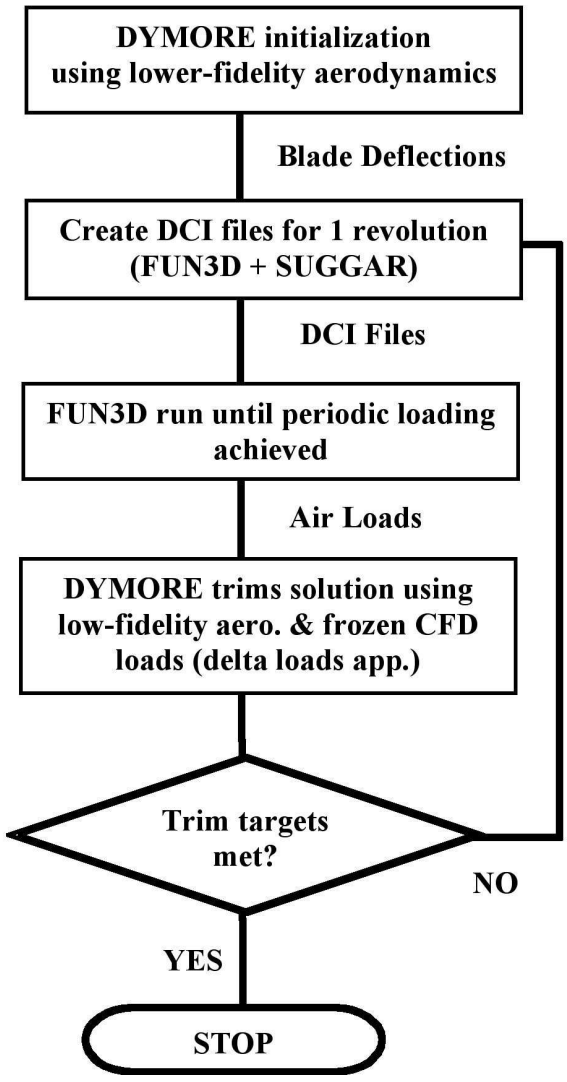

Figure 2: Overset FUN3D–DYMORE Loose Coupling Scheme.

At this point, the loads can be sent back to the CSD

methodology (DYMORE) to evaluate how close to trim the current rotor configuration approaches. Using the delta airloads approach (Ref. 10), the difference between the input CFD and CSD aerodynamic loads is computed. The rotor is then trimmed using a set of input targets (e.g., thrust, pitch and roll hub moments) and one of the lower-fidelity aerodynamics options found in the CSD methodology until a converged solution is obtained. If the targets are predicted within preset tolerances – or the values are no longer changing between iterations – the solution is considered to be "converged to trim". If the computed targets are not within the trim target tolerances, the resulting blade deflections, which implicitly contain the control angles, are passed back to FUN3D where a new set of airloads is computed. As a result trim adjustments that are computed using the DYMORE trimmer at each step are used in the CFD code. This cycle is repeated until a solution that is "converged to trim" is achieved.

This loose-coupling strategy provides solutions that are adequate for many level-flight simulations. Problems have been encountered for flight conditions that have aperiodic loading (highly separated flows) or are located on the edge of the operation envelope. For these flight conditions, as well as maneuvers, a tight-coupling strategy is needed. For the tight-coupling strategy, the previously discussed strategy must occur at a much smaller fraction of the azimuth; updates may be needed within azimuthal changes of one or two degrees in order to capture the transients. For this strategy, the grids and connectivity information will need to be created at each of these updates. Given the current situation where SUGGAR remains an independent code, this process is too user time-intensive to be practical. Two potential solutions to this problem would be to rewrite SUGGAR as a parallel library, as has been done for DiRTLib, or to forgo the utilization of SUGGAR as a facilitator and replace it with routines specific for use in FUN3D.

Test Cases

Georgia Tech Rotor–Fuselage

Experimentalists at Georgia Tech (GT) have performed a series of studies (Ref. 39) for the aerodynamic interaction between a teetering rotor and a simplified fuselage, as shown in Fig. 3. A fuselage consisted of a 0.067m radius and 1.3716m cylinder capped with a hemispherical nose. The rotor was a two-bladed, teetering rigid rotor mounted independently of the fuselage using a strut extending from the ceiling. Each rotor blade consisted of a rectangular planform with a constant, untwisted NACA 0015 airfoil section. The blade radius was 0.4572 m with a 2.7 percent cut out and a chord of 0.086m. The rotor rotation rate was 2100 rpm. The hub was located 1 rotor radius downstream of the nose and 0.3 rotor radii above the fuselage centerline.

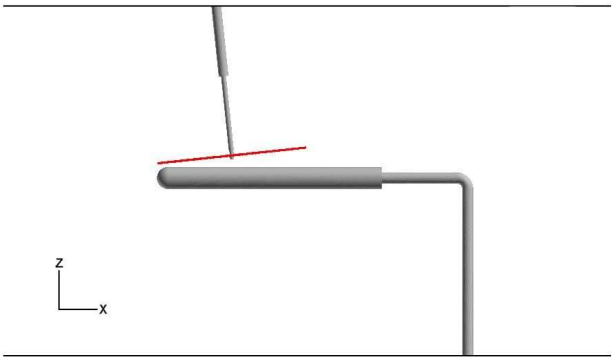

Figure 3: Georgia Tech rotor–fuselage test model (Ref. 16).

An advance ratio of 0.1 with a rotor shaft tilt angle of 6^o and fixed blade pitch of 10^o was chosen for this work. The flap angle defining the blade motion is

$$\theta = -2.02^o sin\psi - 1.94^o cos\psi \qquad (4)$$

For the test case chosen here, the thrust coefficient (C_T) was measured to be 0.00945. It should be noted that the experimental tip path plane shifts to the side since the rotor could not be trimmed given the lack of cyclic pitch control.

The computational grid utilized for this simulation consists of a fuselage grid with 1,870,639 nodes with 36,119 nodes on the fuselage. The overset blade grid consisted of 420,709 nodes and had total 15,784 nodes on the blade surfaces. Therefore, the composite grid had 2,291,348 nodes and 51,903 surface nodes.

UH60A Rotor in Level Forward Flight

The UH60A helicopter flight test database (Ref. 40) has become the correlation standard for CFD-CSD coupling. For illustration here, the high speed case (C8534) has been chosen as the verification case. For the C8534 case, the flight conditions are $\mu = 0.368, \frac{C_T}{\sigma} = 0.084, M_\infty = 0.236, M_t = 0.642, \alpha_s = -7.31^o$, and an altitude of 3273 ft. Target trim values are 17,944 lbs. of thrust, –6884 ft.–lbs. of rolling moment and a 2583 ft.–lbs. of pitching moment. While many of the discrepancies in the data have been resolved (Refs. 41, 42), discrepancies between the thrust and moments from measured and rotor

pressure gauge integrations create uncertainties in the trim condition. Since the experimental mean airload values may be different from computed values, loads are usually shown with the mean values removed.

Each of the UH60's four blades was modeled using its physical properties described in Ref. 43. The blade was modeled using ten cubic beam elements, and the hub-rotor connection was modeled with three segments permitting lag, flap, and pitch rotations. The physical characteristics of the bearing were simulated by springs and dampers in the joints. This structural dynamics model has been correlated within DYMORE and UMARC using experimentally measured airloads and has been previously presented (Refs. 37, 44).

The overset grid utilized for these computations includes five different volumes comprised of tetrahedral elements for the four near-field blade grids and the background grid. There were a total of 18.3 million cells (3.2 million nodes) in the entire grid, with 2.4 million cells (414 thousand nodes) in each blade grid and 8.8 million cells (1.5 million nodes) in the background grid. Fifteen thousand triangles (8000 nodes) were used to model each rotor blade surface, as seen in Fig. 4. The overlay of the near-field blade grid and the background grid is illustrated in Fig. 5. The nearfield blade grid extended about the blade with a 0.22 blade radius, while the outer grid extended outward more than 30 blade radii. Normal spacing at the surface was approximately 1×10^{-6} chords.

Figure 4: FUN3D UH60 blade surface grid.

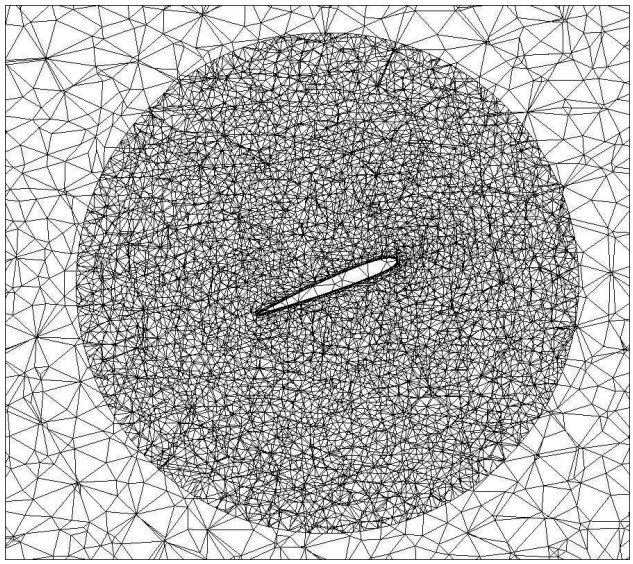

Figure 5: FUN3D UH60 near– and far–field overset grids.

Results

Georgia Tech Rotor–Fuselage

The Georgia Tech rotor–fuselage configuration has been utilized to verify the new rigid body motion routine. Fig. 6 verifies that the implementation of the rigid body motion file is correct for the teetering rotor configuration. Both the overset time-averaged pressure coefficients for the hard-coded motion (Ref. 16) and the motion computed from the rigid body motion module result in the same pressure distribution over the body given the same grid and numerical input selections. In addition to the overset simulations, the results from the unsteady actuator blade (Ref. 16) are included for comparison.

There are some interesting pressure pulses that occur only with the overset computations. Further investigation shows that the tip vortices intersect the fuselage in the areas where the pressure pulses occur. As observed in Fig.7, vorticity from the root area tends travel sharply downward and impinge near the rotor hub ($X/R = 1.0$). The tip vortices travel aft and downward, moving more rapidly downward on the left side, as expected. The influence of the tip vortex as it approaches the fuselage on the left side is first felt about $X/R = 1.5$. When it impinges on the fuselage at about $X/R = 2.3$, the influence is felt around the entire fuselage.

There are no extant data for the rotor blade loads for this configuration. However, if the pressure coefficients for the blade are plotted, as in Fig. 8, one observes that the pressure distributions have the approximate magnitude and shape expected from this airfoil at the estimated angles of attack.

UH60A Blackhawk Rotor

The UH60A Blackhawk rotor is utilized to verify the ability of the unstructured FUN3D code to compute the loads about a rotating system. In order to test the ability of FUN3D without the additional source of error from coupling, a rigid body simulation was run and compared with a comparable OVERFLOW simulation to allow correlation since the experimental data inherently includes flexible blades and is trimmed. Table 1 compares the hub loads for each

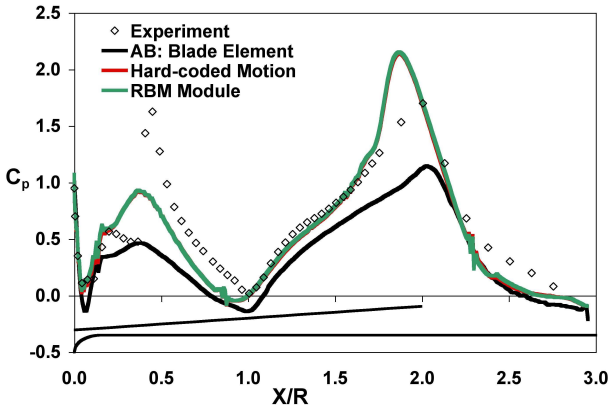

(a) Upper

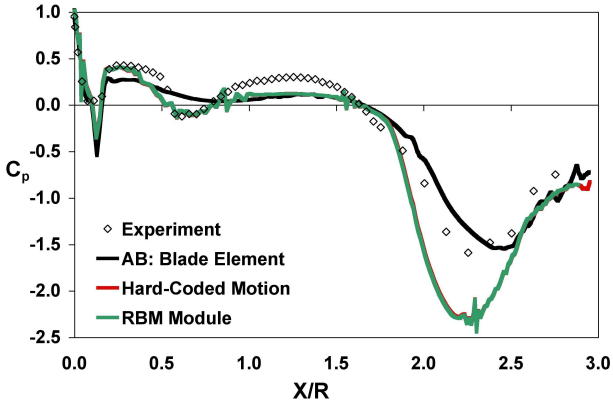

(b) Right

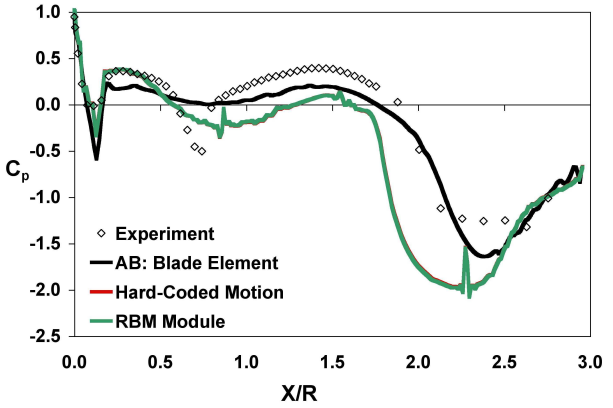

(c) Left

Figure 6: GIT rotor–fuselage time-averaged centerline fuselage pressures.

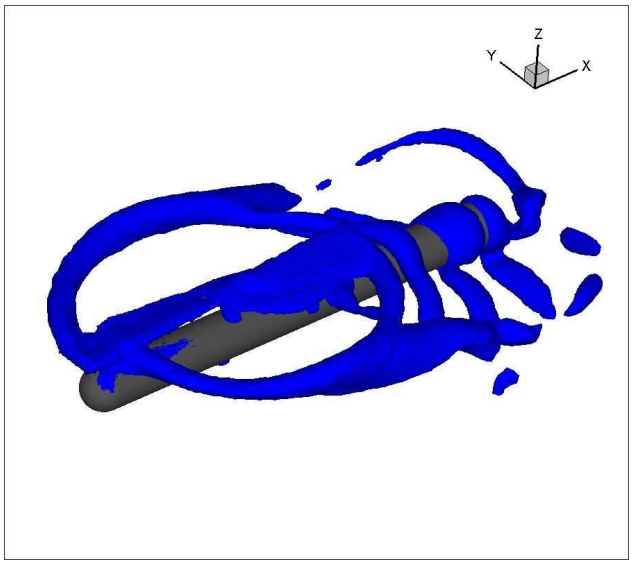

(a) Orthogonal View

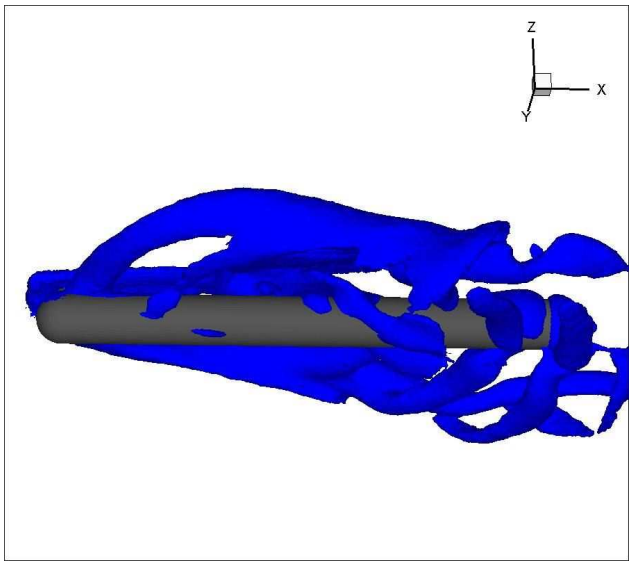

(b) Side View

Figure 7: Wake vorticity for the GIT rotor-fuselage at a $\mu = 0.10$.

simulation, as well as the experimental data. The thrust predictions for the two computational methodologies are very close, within 3% of one another, although there is significant deviation as expected with the experimental data without flexibility or trim. The moment data, which are typically the most sensitive of the integrated parameters, show very large deviations from experiment and one another. The reasons for the integrated moment differences are due to the fact that FUN3D shows a tendency to separate in the third and fourth quadrants, as well as near the tip, as illustrated by the selection of pressure coefficients shown in Fig.9. These pressure coefficients verify that the solution obtained by the FUN3D solver with the overset grids is comparable to its structured

counterpart, OVERFLOW. Although each was run using the Spalart-Allmaras turbulence model, differences in the pressures can be easily accounted for by grid differences and possibly, numerical input selections. FUN3D very closely matches the suction peak predictions for all of the spans examined. Pressure trends throughout the blade disk are very well predicted using OVERFLOW as a guide, and indicate the viability of FUN3D to predict rotor loads.

Proceeding to a flexible simulation (CFD-CSD coupling), the implementation discussed earlier has been tested within FUN3D. Using the DYMORE deflections and controls, the blade is successfully deflected, as illustrated in Fig. 10. If the near-field blade grid remains fixed with respect to the rotor tip path plane so that the blade motion within the near-field grid includes flexibility and rigid motions, care must be taken that the grid outer boundaries remain far enough from the blade so that the grid does not generate unwanted dense spots (e.g., the upper portion of the grid in Fig. 11). If only the elastic motions are updated within the near-field grid, so that the grid moves with the rigid blade motions is another way to alleviate this problem. As illustrated in Fig. 12, the CFD-CSD formulation implemented within FUN3D provides smooth C^o blade deflections, as expected from the physics of the problem.

Conclusions

Advancements in the utilization of unstructured CFD methodologies have been demonstrated via implementations in the FUN3D code. Rigid body motion and CFD-CSD coupling have been demonstrated via several test cases of interest to the rotary-wing community. Preliminary results shown here are comparable to structured overset code results, within the potential errors introduced by differences in the grids. Further research to optimize the domain connectivity information, as well as the most accurate way to update the overset grids needs to be investigated. This work continues to show the viability of unstructured methods for rotary wing applications.

Parameter	Target	OVERFLOW	FUN3D
Blade	Flexible	Rigid	Rigid
Trim	Yes	No	No
F_x (lbs)	—	857	887
F_y (lbs)	—	-507	-940
F_z (lbs)	17944	25445	24472
M_x (ft-lbs)	6884	80266	102238
M_y (ft-lbs)	-2583	5405	96096
t M_z (ft-lbs)	—	-64132	-82951
C_T	0.007247	0.01028	0.009884
$\frac{C_T}{\sigma}$	0.08714	0.1236	0.1204

Table 1: UH60A Integrated parameters from rigid blade simulations.

Acknowledgements

This work is sponsored in part by the National Rotorcraft Technology Center (NTRC) at the Georgia Institute of Technology. Dr. Michael Rutkowski has been the technical monitor of this center. Computational support for the NTRC was provided through the DoD High Performance Computing Centers at MHPCC, ERDC and NAVO through an HPC grant from the US Army. Dr. Roger Strawn is the S/AAA of this grant.. The computer resources of the Department of Defense Major Shared Resource Centers (MSRC) are gratefully acknowledged. The FUN3D Developers Group at NASA Langley Research Center is also acknowledged for their help with FUN3D programming and numerous discussions on rotary-wing modeling. The aid of Dr. David O'Brien of AED in Huntsville, AL to help the first two authors continue in his footsteps is appreciated, as well as the use of his GIT and UH60 blade grids. The late nights debugging and plotting by Mr. Chirag Talati and Mr. Nick Burgess are also much appreciated.

References

[1]Datta, A., Nixon, M., and Chopra, I., "Review of Rotor Loads Prediction with the Emergence of Rotorcraft CFD." *Proceedings of the 31st European Rotorcraft Forum*, Florence, Italy, Sept. 13–15, 2005.

[2]Kunz, D. L., "Comprehensive Rotorcraft Analysis: Past, Present and Future." 46th AIAA/ASME/ASCE/AHS/ASC Structures, Structural Dynamics and Materials Conference, Austin, TX, April 18–21 2005.

[3]Bir, G., and Chopra, I., "Development of UMARC (University of Maryland Advanced Rotorcraft Code)." *Proceedings of the 46th American Helicopter Society Annual Forum*, Washington DC, May 1990.

[4]Johnson, W., "Rotorcraft Dynamics Models for a Comprehensive Analysis." *Proceedings of the 54th American Helicopter Society Annual Forum*, Washington, D.C., May, 20–22 1998.

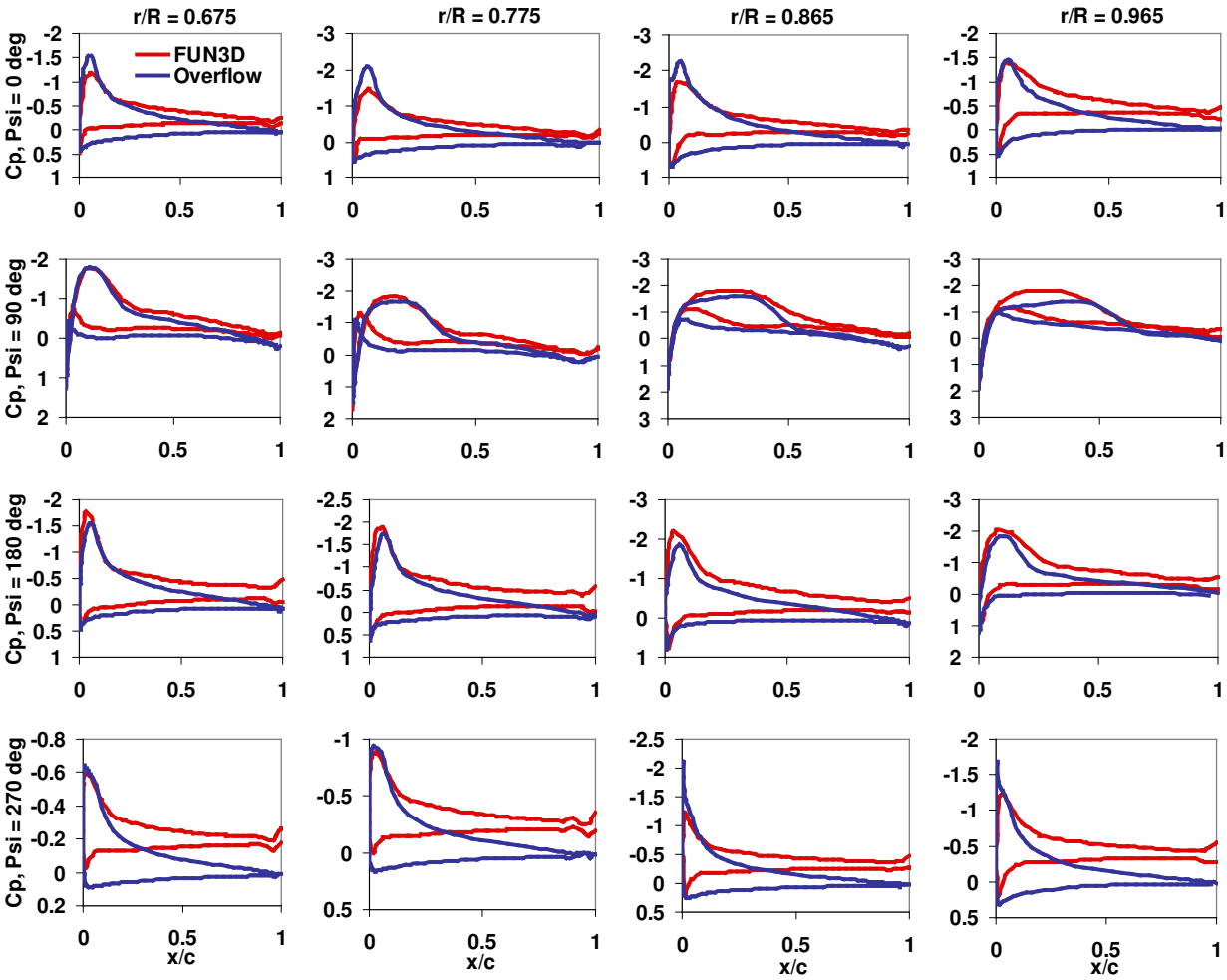

Figure 9: Comparison of FUN3D and OVERFLOW loading for the Case 8534 for UH60A rotor with rigid blades and prescribed motion.

[5]Bauchau, O.A., Bottasso, C.L., and Nikishkov, Y.G., "Modeling Rotorcraft Dynamics with Finite Element Multibody Procedures." *Mathematical and Computer Modeling*, Vol. 33, 2001, pp. 1113–1137.

[6]Beniot, B., Dequin, A., Kampa, K., Grunhagen, W., Basset, P., and Gimonet, B., "HOST, a General Helicopter Simulation Tool for Germany and France." *Proceedings of the American Helicopter Society 56th Annual Forum*, Virginia Beach, Virginia, May, 2–4 2000.

[7]Bridgeman, J. O., Strawn, R. C., Caradonna, F. X., and Chen, C. S., "Advanced Rotor Computations with a Corrected Potential Method." *Proceedings of the 45th Annual American Helicopter Society Forum*, Boston, MA, May 22–24, 1989.

[8]Smith, M. J., *A Fourth-Order Euler/Navier-Stokes Prediction Method for the Aerodynamics and Aeroelasticity of Hovering Rotor Blades*. PhD Dissertation, Georgia Institute of Technology, 1994.

[9]Hodges, D. H., and Dowell, E. H., "Nonlinear Equations of Motion for the Elastic Bending and Torsion of Twisted Nonuniform Rotor Blades." NASA TN D-7818, Dec. 1974.

[10]Potsdam, M., Yeo, H., and Johnson, W., "Rotor Airloads Prediction Using Loose Aerodynamic Structural Coupling." *Proceedings of the American Helicopter Society 60th Annual Forum*, Baltimore, Maryland, June, 7–10 2004.

[11]Georgia Tech/Penn State/Northern Arizona team, "Revolutionary Physics-Based Design Tools for Quiet Helicopters," Final Report, DARPA Helicopter Quieting Program, Dec. 2006.

[12]Makinen, S. et al, "OVERFLOW-RCAS CFD-CSD Coupling." *Proceedings of the American Heli-*

copter Society 62th Annual Forum, Phoenix, Arizona, May 9–11 2006.

[13]Datta, A., and Chopra, I., "Prediction of UH-60A Dynamic Stall Loads in High Altitude Level Flight using CFD/CSD Coupling." *Proceedings of the American Helicopter Society 61st Annual Forum*, Grapevine, Texas, June 1–3, 2005.

[14]Beaumier, P., Costes, M., Rodriguez, B., Poinot, M., Cantaloube, B., "Weak and Strong Coupling Between the elsA CFD Solver and the Host Helicopter Comprehensive Code." *Proceedings of the the 31st European Rotorcraft Forum*, Florence, Italy, Sept. 13–15, 2005.

[15]Ruffin, S., OBrien, D., Smith, M., Hariharan, N., Lee, J., and Sankar, L., Comparison of Rotor-Airframe Interaction Utilizing Overset and Unstructured Grid Techniques, AIAA 2004-0046, AIAA 42nd Aerospace Sciences Meeting, Reno, NV, January 2004.

[16]OBrien, David, *Analysis Of Computational Modeling Techniques For Complete Rotorcraft Configurations*. PhD Dissertation, Georgia Institute of Technology, Advisor: Prof. M. J. Smith, May 2006.

[17]Schweikhard, R. and Le Chuiton, F., "Actuator Disc For Helicopter Rotors In The Unstructured Flow Solver TAU", *Proceedings of the 31st European Rotorcraft Forum*, Florence, Italy, Sept., 2005.

[18]Le Chuiton, F.,"Quasi-Steady Simulation Of A Complete EC-145 Helicopter: Fuselage + Main / Tail Actuator Discs + Engines", *Proceedings of the 31st European Rotorcraft Forum*, Florence, Italy, Sept., 2005.

[19]Heise, R. and Meyer, C. J. and von Backstrom, T. W., "Development Of A Method For CFD Evaluation Of Helicopter Fuselages," *Proceedings of the 31st European Rotorcraft Forum*, Florence, Italy, Sept., 2005.

[20]Renaud, T., OBrien, D., Smith, M. and Potsdam, M., Evaluation Of Isolated Fuselage And Rotor-Fuselage Interaction Using CFD, *Proceedings of the American Helicopter Society 60th Annual Forum*, Baltimore, MD, June, 2004.

[21]Hariharan, N., *High Order Simulation of Unsteady Compressible Flows Over Interacting Bodies with Overset Grids*, Ph.D. Thesis, School of Aerospace Engineering, Georgia Institute of Technology, Atlanta, GA, 1995.

[22]OBrien, D., M., and Smith, M. J., Understanding The Physical Implications Of Approximate Rotor Methods Using An Unstructured CFD Method, *Proceedings of the 31st European Rotorcraft Forum*, Florence, Italy, September, 2005.

[23]Park, Y. and Kwon, O., Simulation of Unsteady Rotor Flow Fields Using Unstructured Sliding Meshes, *Proceedings of the American Helicopter Society 58th Annual Forum*, Montreal, Canada, June 2002.

[24]Park, Y., Nam, H., and Kwon, O., Simulation of Unsteady Rotor-Fuselage Interactions Using Unstructured Adaptive Meshes, *Proceedings of the American Helicopter Society 59th Annual Forum*, Phoenix, AZ, May 2003.

[25]Duque, E., Sankar, L. , Menon, S., Bauchau, O.. Ruffin, S., Smith, M., Ahuja, K., Brentner, K. , Long, L., Morris, P., and Gandhi, F., AIAA-2006-1068, 44th AIAA Aerospace Sciences Meeting and Exhibit, Reno, Nevada, Jan. 9–12, 2006

[26]Bonhaus, D., *An Upwind Multigrid Method For Solving Viscous Flows On Unstructured Triangular Meshes*, M.S. Thesis, George Washington University, 1993.

[27]Anderson, W., Rausch, R., and Bonhaus, D., Implicit/Multigrid Algorithms for Incompressible Turbulent Flows on Unstructured Grids, *Journal of Computational Physics*, Vol. 128, No. 2, 1996, pp. 391-408.

[28]Biedron, R., Vatsa, V., and Atkins, H., Simulation of Unsteady Flows Using an Unstructured Navier-Stokes Solver on Moving and Stationary Grids, 23rd AIAA Applied Aerodynamics Conference, Toronto, Canada, June 2005.

[29]Chorin, A., A Numerical Method for Solving Incompressible Viscous Flow Problems, *Journal of Computational Physics*, Vol. 2, No. 1, 1967, pp. 12-26.

[30]Roe, P., Approximate Riemann Solvers, Parameter Vectors, and Difference Schemes, *Journal of Computational Physics*, Vol. 43, Oct. 1981, pp. 357-371.

[31]Noack, R., DiRTlib: A Library to Add an Overset Capability to Your Flow Solver, 17th AIAA Computational Fluid Dynamics Conference, Toronto, Canada, June 2005.

[32]Noack, R., SUGGAR: A General Capability for Moving Body Overset Grid Assembly, 17th AIAA Computational Fluid Dynamics Conference, Toronto, Canada, June 2005.

[33]Berdichevsky,V.L. , "On the energy of an elastic rod." *Journal of Applied Mathematics and Mechanics* , Vol. 45, 1982, pp. 518–529.

[34]Cesnik, C.E.S., and Hodges, D.H., "VABS: a new concept for composite rotor blade cross-sectional modeling." *Journal of the American Helicopter Society*, Vol. 42 (1), January 1997, pp. 27–38.

[35]Bauchau, O.A. , Choi, J.Y., and Bottasso, C.L., "On the modeling of shells in multibody dynamics." *Multibody System Dynamics*, Vol. 8 (4), 2002, pp. 459–489.

[36]Peters, D. and Barwey, D., "A General Theory of Rotorcraft Trim," *Mathematical Problems in Engineering*, Vol. 2, 1996 pp. 1–34.

[37]Abras, J., Smith, M., and Bauchau, O., Rotor Airload Predictions Using Coupled Finite Element and Free Wake Methods, *Proceedings of the AHS 62nd Annual Forum*, Phoenix, AZ, May 2006.

[38]Nygaard, T.A., Saberi, H., Ormiston, R., Strawn, R.C., Potsdam, M., and Johnson, W., "Fluid Structure Interface for Rotorcraft Aeromechanic Computations." *Unpublished*, 2005.

[39]Brand, A., *An Experimental Investigation of the Interaction Between a Model Rotor and Airframe in Forward Flight*, Ph.D. Thesis, Georgia Institute of Technology, 1989.

[40]Kufeld, R. M., Balough, D. L., Cross, J. L., Studebaker, K. F., Jennison, C. D., and Bousman, W. G., "Flight Testing of the UH-60A Airloads Aircraft," *Proceedings of the American Helicopter Society 50th Annual Forum*, Washington, D.C., May, 1994.

[41]Bousman, W. G., and Kufeld, R. M., "UH-60A Airloads Catalog." NASA TM 212827, August 2005.

[42]Kufeld, R. M. and Bousman, W. G.,"UH-60A Airloads Program Azimuth Reference Correction." Technical note, *Journal of the American Helicopter Society*, Vol. 50 (2), April 2005, pp. 211–213.

[43]Bousman, W., "An Investigation of Helicopter Rotor Blade Flap Vibratory Loads." *Proceedings of the 48th American Helicopter Society Annual Forum* , Washington, D.C., June 1992.

[44]Datta, A., and Chopra, I., "Validation of Structural and Aerodynamic Modeling Using UH-60A Flight Test Data." American Helicopter Society 59th Annual Forum, Phoenix, Arizona, May 6–8, 2003.

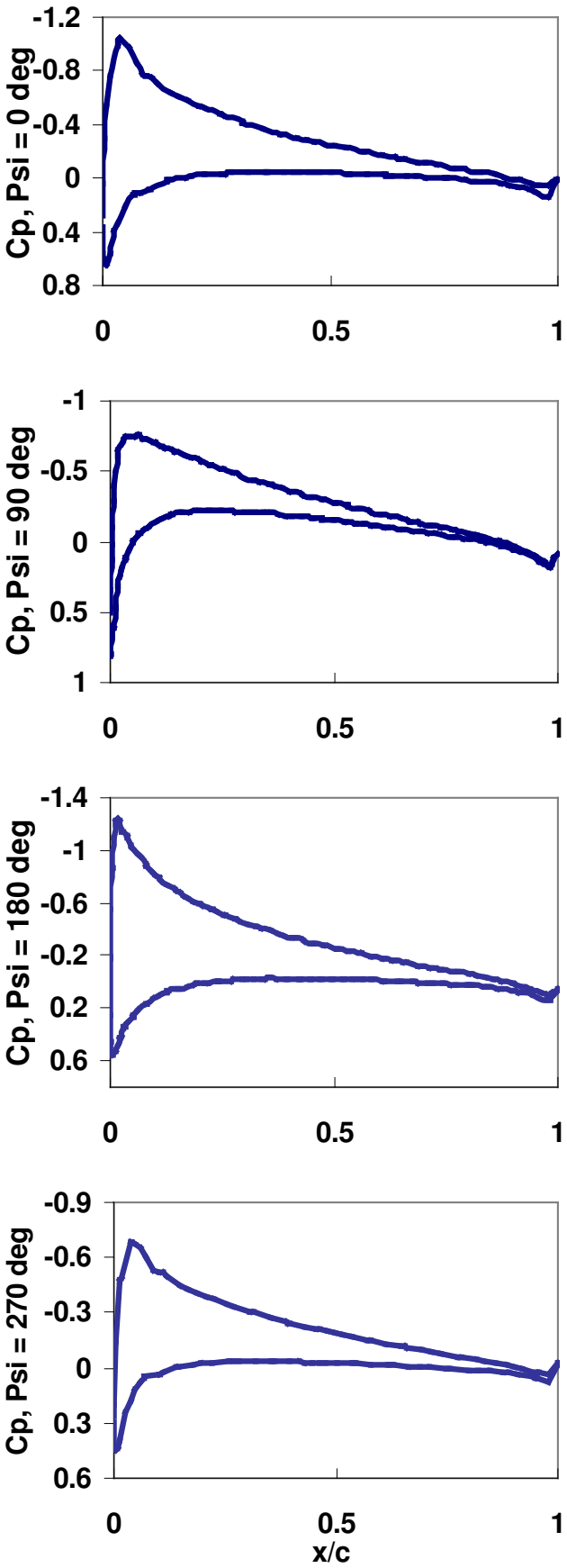

Figure 8: Pressure coefficients for the GIT rotor at a $\mu = 0.10$.

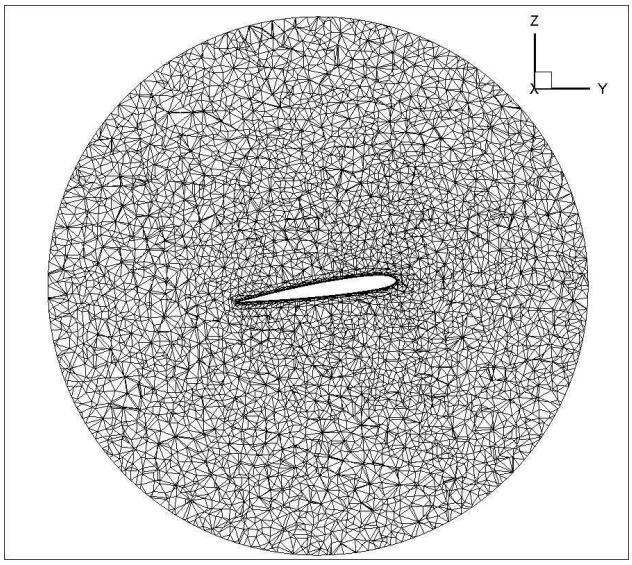

(a) Undeflected grid

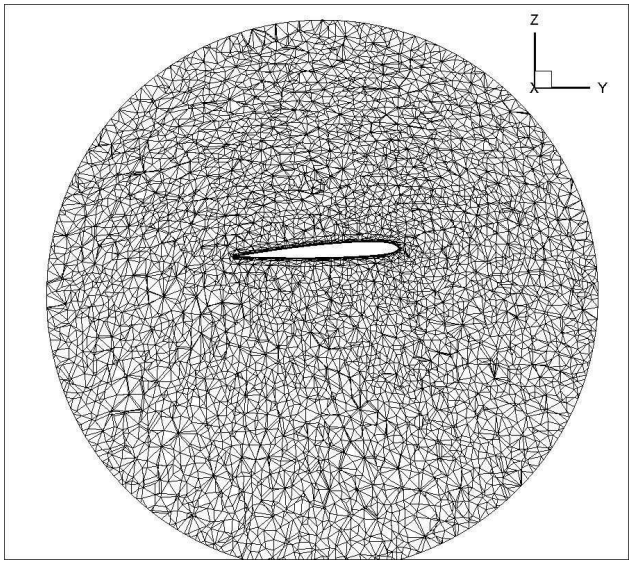

(b) Deflected grid

Figure 10: Comparison of an undeflected and deflected blade grid.

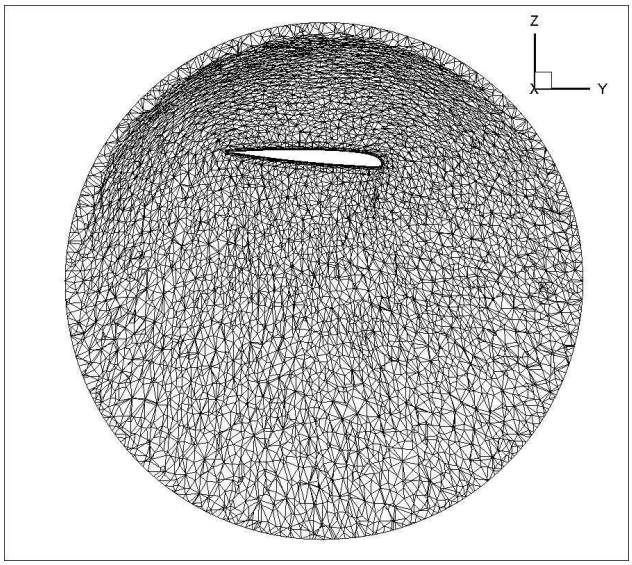

Figure 11: Large blade deflections along with rigid blade motions can cause problems in a deforming grid.

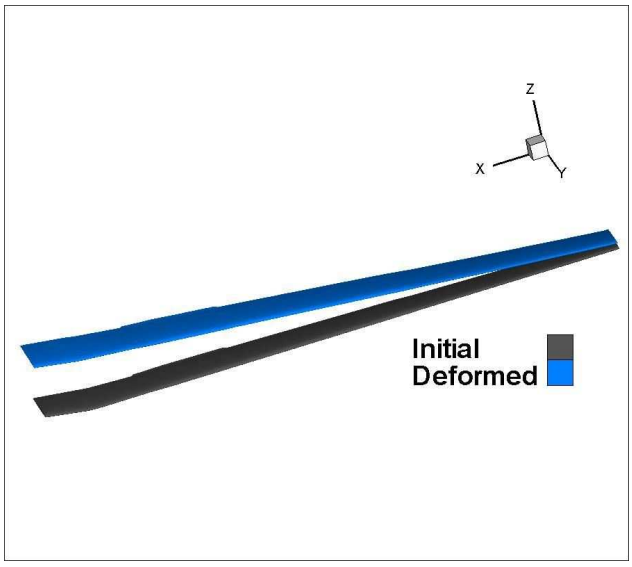

Figure 12: Comparison of an undeflected and deflected blade surface.